Artificial neural network based dynamic dump load control for integrated standalone microgrid

Anand Kumar Myla[1]*, *Srinivasa Rao* Gorantla[1]

[1]Electrical and Electronics Engineering Department, Vignan's Foundation for Science, Technology and Research, Vadlamudi, Guntur-522213, India.

Abstract. ANN control approach for DC-link stabilization and power flow coordination in a standalone hybrid microgrid formed by a 10 kWp photovoltaic array, a 20 kW wind turbine generator, and a 60 kWh battery storage system operating on a 600 V bus. A controllable dump-load branch is integrated into the design to dissipate surplus energy when the battery reaches its upper state-of-charge limit. The ANN dynamically generates converter duty ratios based on its inputs of DC-link error, its rate of change, and real-time renewable power. Simulation studies conducted in MATLAB demonstrate that the proposed controller maintains DC-link variations within ±2 %, reduces voltage ripple to approximately 3.2 V, and limits current distortion to 2.64 %, while a PI controller exhibits slower recovery, higher overshoot, and post-filter harmonics of about 3.82 %. The results confirm that ANN-based dump-load coordination ensures stable operation, prevents converter stress due to power surplus, and improves the overall utilization of renewable energy in standalone microgrid environments.

1 Introduction

The need to have sustainable and decentralized energy systems has led to the creation of standalone hybrid microgrid which incorporates renewable energy system like solar photovoltaic(SPV) arrays and wind turbine generators(WTG) with battery energy storage systems(BESS). These are pictured systems which will be crucial in rendering dependable power to remote or islanded regions which have restricted or no access to the grid [1-3]. Although they present the benefits of operational cleanliness and resource diversity, hybrid standalone microgrid also are characterized by operational challenges which can be traced to intermittency and nonlinear nature of the renewable resource. Surging load changes caused by the fast variation in the amount of solar irradiance or wind speed lead to DC link voltage variations, converter stress, frequency variations and, hence, poor power quality [4-6].

The DC bus is used to form a central point of energy sources and loads in a hybrid microgrid. A stabilized DC voltage is a must when operating converters and what makes the equipment safe [7, 8]. The changes in the output of renewable sources rapidly or the maturity of charged batteries can raise the accumulation of energy in the DC bus, which will result in overvoltage. On the other hand, due to low renewable output, undervoltage scenario might

* Corresponding author: anandmyla2019@gmail.com

occur, which negatively affects inverter operations and the voltage regulation of the AC output [9].

Such issues demonstrate the need to have advanced control methods that can dynamically stabilize the DC link voltage and coordinate the power flow in between renewable sources, storage and loads. Proportional-integral (PI) controllers are often used in renewable microgrid because they are simple to set up. But their fixed parameters mean they don't work as well in conditions that change over time. Large environmental changes cause slow response. PI controllers also don't reduce harmonics well, causing distortion and unstable voltage regulation. To fix these problems, researchers have studied methods like fuzzy logic control, model predictive control, and artificial neural nets (ANNs) [10, 11]. ANNs are of interest because of their learning ability, mapping efficiency, and adaptive tuning, which reduces the need for math models [12].

A major gap in the available literature is that most of the ANN or intelligent controllers designed so far for converter-level voltage regulation or MPPT functions for such systems do not address the surplus energy dissipation problem after a BESS gets fully charged [13]. Under such conditions, continued renewable generation may increase the DC-link voltage beyond its nominal value and result in thermal and electrical stress on power converters. For mitigating this issue, a DC-link dynamic dump-load mechanism can be deployed to absorb excess power and maintain the stability of the voltage bus. Similarly, integrating an adaptive ANN controller with such a mechanism promises a very effective approach for achieving balanced operation and improved power quality in standalone hybrid microgrid [14, 15]. Motivated from the above discussions, in this work, an artificial neural network-based adaptive control approach has been proposed for a hybrid SPV-WTG-BESS standalone microgrid interfaced with a DC-link dynamic dump-load mechanism. The proposed controller continuously monitors the DC-link voltage error, its rate of change, and power flow between the renewable and storage subsystems for regulating converter duty ratios in real time. By coordinating the SPV, WTG, BESS, and dump-load converters adaptively, the ANN ensures rapid transient recovery, minimized voltage ripple, and reduced harmonic distortion. It perfectly balances energy under varying environmental and load conditions without requiring any manual gain tuning.

The main contributions of this work are as follows. An ANN-based adaptive control scheme is developed to regulate the DC-link voltage in real time for a integrated standalone microgrid combining solar, wind, and battery systems. A DC-link dynamic dump-load mechanism is added to absorb extra energy and prevent overvoltage when generation is high and the battery is fully charged. The ANN uses an adaptive learning rule that updates control parameters automatically without any offline training or manual tuning. Simulation results show that the proposed ANN controller performs better than the conventional PI controller in maintaining voltage stability, improving transient response, and reducing current harmonics under changing renewable and load conditions.

The remainder of this paper is organized as follows: Section 2 presents the configuration and mathematical modeling of the SPV–WTG–BESS integrated system along with the DC-link dynamic-load design. Section 3 details the proposed ANN-based adaptive control strategy and its learning mechanism. Section 4 gives the outcomes of the system, and comparative analysis, while Section 5 concludes the work with key findings and future scope of the work.

2 System configuration for the microgrid

Proposed into the mix is what we have labeled a standalone hybrid microgrid which includes a solar photovoltaic (SPV) array, a wind turbine generator (WTG) which in this case uses a Doubly Fed Induction Generator (DFIG), a battery energy storage system (BESS) and also a

DC link dynamic load (dump load) controller as seen in Fig. 1. This system puts out regulated AC power through a voltage source inverter (VSI) to isolated loads which at the same time are subject to changing environmental conditions. We put forward that it's to maintain DC link voltage stability, to get sources and storage to play nice and coordinate their output, and to get total harmonic distortion (THD) levels in at or below the IEEE 519-2014 standards.

The integrated architecture follows a DC-coupled topology in which the SPV and WTG subsystems interface a common DC-link through individual DC–DC converters. The BESS connects via a bidirectional converter that supports both charging and discharging operation, while a controllable resistive branch—termed the DC-link dynamic-load or dump-load—is connected in parallel with the DC bus to dissipate surplus energy during high-generation conditions.

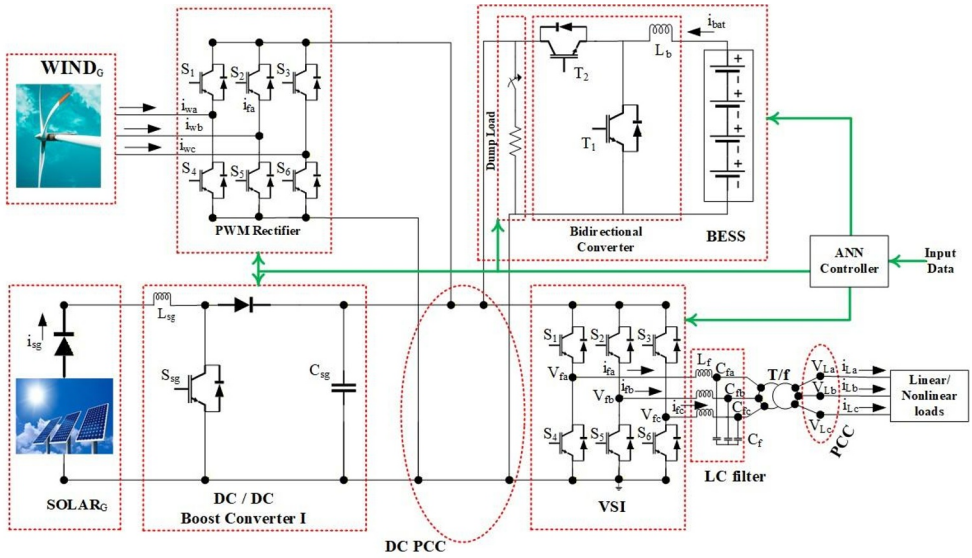

Fig. 1. Block diagram of the Microgrid system.

$$I_{PV} = I_{ph} - I_0 \left[\exp\left(\frac{(q(V_{PV}+ I_{PV}R_S))}{n\,k\,T}\right) - 1\right] - \frac{V_{PV}+ I_{PV}R_S}{R_{sh}} \quad (1)$$

where Iph is the photocurrent dependent on irradiance, I_o is the diode reverse-saturation current, q is the electron charge, n is the ideality factor, k is Boltzmann's constant, T is the cell temperature, and R_s, R_{sh} are series and shunt resistances respectively . The ANN-based MPPT algorithm continuously perturbs the duty cycle of the DC-DC boost converter to maintain operation at the maximum power point under variable irradiance [2].

The 20 kW WTG subsystem converts aerodynamic energy from wind into electrical power through a doubly-fed induction generator. The mechanical power captured by the turbine is [13], [14]:

$$P_w = 0.5 * \rho * A * C_{p(\lambda,\beta)} * v_w^3 \quad (2)$$

where ρ is the air density, A is the rotor swept area, Cp is the power coefficient depending on tip-speed ratio (λ) and pitch angle (β), and vw is the instantaneous wind velocity. A three-phase diode rectifier converts the generator output to DC, followed by a boost converter that regulates the DC-link voltage in coordination with the ANN controller.

The 60 kWh BESS provides energy balancing between generation and load, operating in charge or discharge mode through a bidirectional DC-DC converter. The BESS voltage and state-of-charge are expressed as [10],

$$V_{bat} = E_{bat} - I_{bat} * R_{int} \quad (3)$$

$$SOC(t) = SOC(0) - \left(\frac{1}{C_{bat}}\right) * \int I_{bat} dt \quad (4)$$

where Ebat is open-circuit voltage, Rint internal resistance, and Cbat capacity. Charging occurs when Pbat < 0; discharging occurs when Pbat > 0. The controller maintains SOC within 20–95 % to prevent deep cycling. [10]. The converter controller maintains the DC-link at its reference of 600 V by adjusting the battery current reference generated by the ANN algorithm [2].

Under steady operation the instantaneous power balance across the DC link satisfies [1, 4]:

$$P_{pv} + P_{wt} + P_{bat} = P_{load} + P_{loss} + P_{dump} \quad (5)$$

where Ppv and Pwt are powers from SPV and WTG, Pbat is BESS power (positive on discharge), Pload is load power, Ploss converter losses, and Pdump dump-load dissipation. This equation ensures instantaneous power equilibrium and forms the basis for ANN training to maintain steady DC-bus voltage under dynamic operating conditions.

During conditions of high renewable generation and nearly full battery charge, the DC-link voltage tends to rise above its reference Vdc,ref. To limit this, the DC-link dynamic-load branch automatically dissipates excess energy. The instantaneous dissipated power is

$$P_{dump} = \frac{V_{dc}^2}{R_{dump}} \quad (6)$$

Its control law is based on the voltage error

$$e_{dc(t)} = V_{dc},ref - V_{dc(t)} \quad (7)$$

The ANN adjusts the chopper duty ratio Ddump to minimize edc(t), increasing dissipation when Vdc > Vdc,ref .

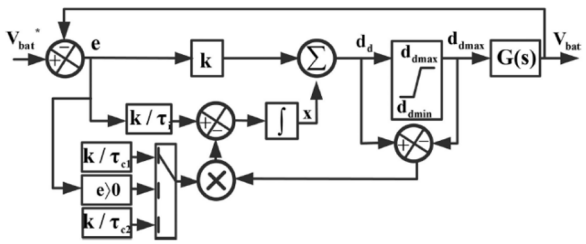

Fig. 2. DC Dump Load Control Mechanism [7].

Fig. 2 illustrates the DC dump-load control structure adopted to maintain the voltage stability of the battery bus under varying generation and storage conditions. The controller values the immediate battery voltage and calculates their variation with respect to its reference in order to produce a control error signal. This error signal goes through a proportional-integral compensator that modulates the duty ratio of the dump converter. Using anti -wind-up protection, the system limits the duty cycle to pre-defined limits and reduces overshoot when

experiencing abrupt transients. To limit the DC dumping to its maximum available energy, when the DC-linked voltage exceeds the threshold the control loop extends the dump-load conduction period and causes the problem of excess energy dissipation and the voltage to return to its nominal value. When equilibrium is reached, the ratio of the duty is slowly restored to its lower limit, thus, the recovery of the voltage is smooth, and the converters are not subjected to high levels of stress during high-generation periods.

The supervisory artificial neural network gets as inputs the variables: edc, e dicembre, Ppv, Pwt and SOC and produces the ratios of duty that should be added to the SPV, WTG, BESS and dump-load converters.

$$\left[D_{pv},\ D_{wt},\ D_{bat},\ D_{dump}\right] = f_{ANN(e_{dc},\dot{e}_{dc},P_{pv},P_{wt},SOC)} \tag{8}$$

The ANN controller implements real-time coordination of power-flow on the substystems. When the renewable production is not enough (Ppv + Pwt less than Pload) the battery is discharged to assist the DC-link. The battery is charged in case of moderate surplus power and SOC is below 95%. When the generation is large and the battery charged (SOC 95 percent or more), the dump-load will start to dissipate energy, and the DC voltage will be held constant at its reference. This top-down decision making process eases the transition over and discourages volatile changes. The joint modeling and control of the integrated SPV–WTG-BESS standalone microgrid provides steady DC-link control, controlled energy sharing and unwanted harmonic distortion. To maintain the necessary voltage and power balance, the ANN also keeps the duty ratios in real time, thus eliminating the human intervention and wrapping up the requirements of IEEE 519-2014 and IEEE 1547-2018 requirements. The following chapters introduce the environment of simulation and show the results of the proposed ANN-based control system compared to the conventional PI controller. This synchronized modeling to allow is to perform flexible regulation of voltages and active load sharing through renewable, storage, and dump pathways, the foundation of the ANN controller in the coming section.

3 ANN control methodology

The intelligent control system for the hybrid SPV–WTG–BESS microgrid relies on an artificial neural network (ANN). This network learns the relationships between power generation, storage, and load changes, as seen in Fig. 3. Instead of using fixed proportional-integral control, this controller uses an adaptive method that responds to voltage changes and system disturbances in real time. The main purpose is to manage the DC-link voltage, organize converter power flow, and keep harmonic levels within the IEEE 519-2014 limits, while also keeping steady-state error low. The design of the controller is based on the immediate DC-link voltage error and its integral, which shows how much the actual voltage varies from the target voltage [1, 5]. The two inputs are defined as

$$e_v(t) = V_{dc\_ref} - V_{dc}(t) \tag{9}$$

and the rate of change of error as

$$\dot{e}_{dc(t)} = \frac{de_{dc(t)}}{dt} \tag{10}$$

These values show the temporary state of the DC bus. Inputs like real-time solar power (Ppv), wind power (Pwt), and battery SOC give background on the microgrid's changing

state. The artificial neural network (ANN) works through a feed-forward arrangement that includes a hidden layer and a hyperbolic-tangent activation function. The way each neuron's output is calculated can be described as

$$y_j = \tanh\left(\Sigma_i \left(w_{ji} * x_i\right) + b_j\right) \tag{11}$$

where wji represents the weight of the connection between input i and neuron j, xi is the normalized input, and bj stands for the bias term. After a linear change in the output layer, the end control signals are produced, which are appropriate for the constant changes needed for converter duty ratios.

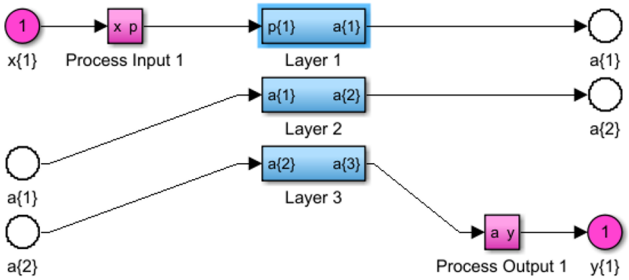

Fig. 3. Simulation subsystem of ANN Controller.

The controller is trained online using a gradient-descent rule that minimizes the instantaneous cost function [14]:

$$J(t) = \tfrac{1}{2} w e_{dc}^2(t) + \tfrac{1}{2} \lambda W(t)^2 \tag{12}$$

where ω denotes the voltage error weight and λ is a small regularization gain for smooth ANN adaptation.

The weight update law is

$$w_{i(t+1)} = w_{i(t)} - \eta * \frac{\partial J(t)}{\partial w_i} \tag{13}$$

where η represents the adaptive learning rate. To ensure fast convergence during transients and stability near equilibrium, the learning rate varies according to [9], [10].

$$\eta(t) = \eta_{\min + (\eta_{\max} - \eta_{min})} * \frac{\left|e_{dc(t)}\right|}{V_{dc}, ref} \tag{14}$$

This adaptive formulation accelerates learning when large voltage deviations occur and refines control precision as the error diminishes. Because the algorithm operates continuously, the network weights evolve smoothly with system dynamics and eliminate the need for offline training or gain retuning. The ANN interacts directly with the DC-DC and DC-AC converter stages. For the photovoltaic and wind channels, the controller regulates the converter duty ratios to extract maximum power while maintaining DC-bus equilibrium. The battery converter operates bidirectionally: it discharges whenever the combined renewable generation is insufficient and charges when a power surplus exists. When the BESS reaches its upper state-of-charge threshold and renewable power continues to exceed load demand, the DC-link voltage begins to rise. At that instant the ANN activates the DC-link dynamic-

load path by increasing the chopper duty ratio Ddump. The dissipated power is given in eq (6), and the control law given in eq (7). so that the surplus energy is converted into heat in the resistive branch until the voltage returns to nominal value. When balance is reached, the ANN slowly lowers Ddump to zero. This stops swings or needless waste. This flexible way of controlling the dump load works with the battery-energy-management loop. Artificial neural network (ANN) is used to predict the training of the intelligent control system of the hybrid SPV-WTG-BESS microgrid to identify the interdependence among the variations in power generation, energy storage, and load as shown in Fig. 3. Instead of using standard fixed proportional-integral controllers, the controller uses an adaptive approach that can respond to real-time changes in voltages and system upsets. Its main goal is to control the DC-link voltage, coordinate converter power flows, and to do harmonic distortion within the bounds of the IEEE519-2014, and at the same time to maintain a low steady-state error [15].

The controller design is based on the error of the DC -link voltage instantaneous and the error of its integration, so as to measure the difference between the real voltage and the specified voltage [1, 5]. The two input signals are what can be stated in the following:

$$V(t) = 0.5 * e_{dc}^{2(t)} \tag{15}$$

whose derivative satisfies,

$$\frac{dV}{dt} = e_{dc} * \dot{e}_{dc} = -k * e_{dc}^{2(t)} < 0 \tag{16}$$

The controller goes further to protect the converter during the times when the generation output is high. The acquisition of the voltage, current and SOC measurements starts each control cycle. These variables are standardized and passed on to ANN, which calculates new duty ratios. The resulting duty ratios are passed to a pulse-width-modulation (PWM) interface that aligns the signals of the gate of all the converters. After the switch operation, the ANN measures the DC-link voltage, compares it to the new error and readjusts its internal weights to reduce the resulting costing function:

$$U(t) = f_{ANN}\left(e_{dc(t)}, \dot{e}_{dc(t)}, P_{pv(t)}, P_{wt(t)}, SOC(t)\right) \tag{17}$$

where $f_{ANN}(\cdot)$ represents the nonlinear mapping realized by the trained model. The functionality is constantly changed with changes in operating conditions so that it will guarantee real-time coordination of renewable inputs, battery flow, and dump-load activity. The controller decreases Dump and orders battery discharge when the renewable generation decreases and vice versa. A smooth change between those modes is provided, and thus eliminates DC -bus oscillations and increases the power-quality indices at the inverter output. To determine the instant energy balance of the renewable generation, load demanded, and the state of charge (SOC) of the 60 kWh battery, the hybrid microgrid operates in several modes. The ANN controller optimally varies control measures to stabilize the DC -link voltage and maximize renewable power use. Table1 summarizes the operation modes under different conditions of power-flow.

The ANN decision process was implemented using a real-time sequence of operations rather than a static mapping. At each control interval, the system retrieves a fresh set of measurements consisting of DC-link voltage, its rate of change, power from SPV and WTG, and the BESS state-of-charge. These inputs form the input vector fed to the feed-forward network. The hidden layer applies non-linear activation to capture the correlation between sudden renewable variations and corresponding DC-link deviations. The output layer computes the required duty cycle values for all converters. The generated PWM signals are

then used to drive the converter switches. The loop is continuously repeated, and the network parameters are refined using a gradient-descent update, allowing the controller to learn without offline retraining.

Pseudo-Algorithm: ANN-Based Dump Load Control

1. Read Vdc, SOC, Ppv, Pwt and compute error and change in error.
2. Normalize inputs and feed them to the ANN.
3. Evaluate hidden layer activation and compute output duty ratios.
4. Apply duty ratios to SPV, WTG, and BESS converters.
5. If SOC ≥ SOCmax and Vdc > Vref: Increase Ddump and dissipate surplus energy.
6. If Vdc approaches Vref: Gradually reduce Ddump to prevent oscillation.
7. Update network weights using the error-based cost function.
8. Repeat for every sampling period.

Table 1. Various working Modes of the Proposed System.

Mode	Operating Condition	Available Sources	Battery Status
Mode 1 – Normal Charging	SOC > 50 % and (PPV + PWT > PL)	PV, WT, Battery	Charging
Mode 2 – Discharging	SOC > 50 % and (PPV + PWT < PL)	PV, WT, Battery	Discharging
Mode 3 – Low SOC Charging	SOC < 50 % and (PPV + PWT > PL)	PV, WT, Battery	Charging
Mode 4 – Full Charge / Dump Load	SOC = 100 % and (PPV + PWT > PL)	PV, WT, Dump Load	Charging stopped
Mode 5 – Low Renewable Support	SOC < 50 % and (PPV + PWT < PL)	PV, WT, Battery	Discharging

In Mode1, the battery would experience a controlled charging regime whenever the renewable generation exceeds the load demand, thus ensuring that it conserves a lot of energy and reduces harmonic distortion. Mode 2 assumes intermediate renewable conditions, where the battery is discharged to assist the load to keep the DC -link stable. Once battery state of charge (SOC) decreases to less than 50 per cent, Mode 3 is activated so that whenever excess renewable energy is detected it will recharge the battery. Mode 4 Once the battery reaches full capacity (SOC 100 per cent), the DC dump load is activated to absorb the surplus power and consequently avoid overcharging. Lastly, Mode 5 is activated whenever there are extended periods of low-generation where the battery and renewable ones conserve continuity of supply. Depending on the instantaneous balance of power and SOC of the battery, the artificial neural network controller controls the microgrid by switching between these two different operating modes as shown in Table 1.

4 Simulation Results and Discussion

The ANN-based DC dump load control method was tested in MATLAB Model using changing solar light, different wind speeds, and irregular load changes. The system includes a $10\,^{kW_P}$ PV array, a 20 kW DFIG wind turbine, a 60 kWh battery, and a 120 Ω DC dump load, all linked through a 600 V DC connection as shown in Fig. 4

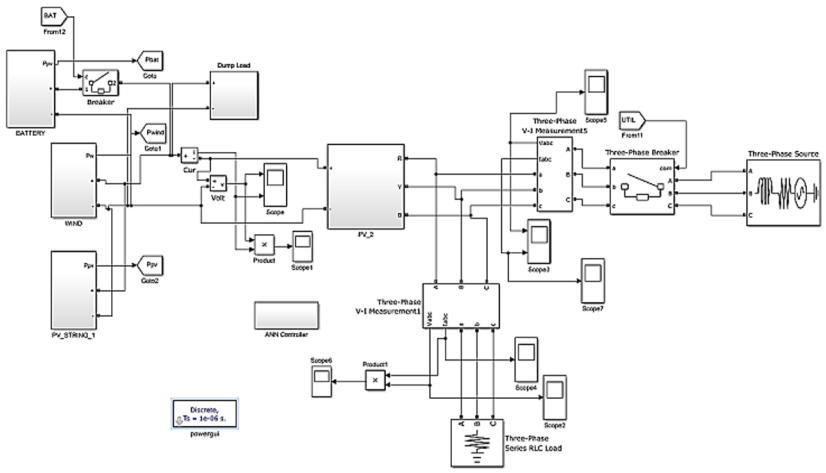

Fig. 4. Simulation circuit of Microgrid system.

The simulation settings are based on those in Table 2 of the system design part, which makes sure there is a practical balance between renewable energy input and load needs. The solar array was tested under irradiance levels of 400, 600, 800, and 1000 W/m² at 25°C. The resulting I–V and P–V curves demonstrate the nonlinear nature of photovoltaic output and the influence of irradiance on maximum power point (MPP) tracking. The ANN-controlled converter maintains operation at MPP even during sharp irradiance transitions.

Table 2. Simulation parameters of the Microgrid system.

Parameter	Value / Type
DC-link reference voltage	600 V
Solar photovoltaic array	10 kW_P
Wind turbine generator	20 kW
Battery energy storage system	1250Ah (60 kWh)
Battery nominal voltage	48 V
Load (three-phase nonlinear)	10 kW
Filter inductance	2 mH
Filter capacitance	100 μF
Inverter switching frequency	10 kHz
Simulation sampling time	1 ms
Learning rate	0.001
Nominal proportional gain	0.04
Nominal integral gain	8
Rdump	120 Ω

The proportional-integral controller was tuned by applying a classical step-response approach on the DC-link subsystem under nominal irradiance and average wind speed. In detail, the proportional gain was increased until a sustained oscillation was observed and then reduced to a stable value; subsequently, the integral gain was tuned to eliminate steady-state error without overshoot. The resulting parameters used throughout all simulations are KP = 0.04 and KI = 8.0, which provided stable operation in the absence of sudden renewable surges.

The I–V and P–V curves of the 10 kW_P solar PV array were obtained for irradiance levels varying from 200 W/m² to 1000 W/m² at 25 °C. The array, composed of 19 series and 2 parallel modules (each 305 W), exhibits a nominal DC-link voltage of approximately 600

V. As shown in Fig. 5, the current remains almost constant with voltage up to the knee region, after which it rapidly decreases near open-circuit conditions. The corresponding P–V curves illustrate a single prominent maximum for each irradiance level, confirming stable MPP tracking behavior. The smooth and linear increase of power with irradiance validates the proper functioning and scaling of the PV subsystem integrated into the hybrid microgrid framework.

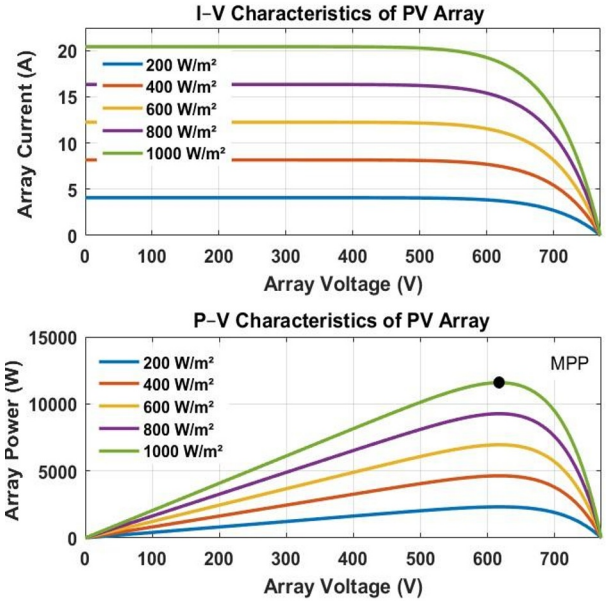

Fig. 5. I–V and P–V Curves.

Fig. 6 illustrates the aerodynamic and delivered electrical power characteristics of the 20 kW DFIG wind turbine. The turbine begins generating power once the wind speed exceeds the cut-in value of 3.2 m/s, following a cubic relationship between power and velocity. As the wind speed approaches the rated value of 12 m/s, the output smoothly transitions to its nominal 20 kW capacity, demonstrating the pitch-controlled soft-knee behavior.

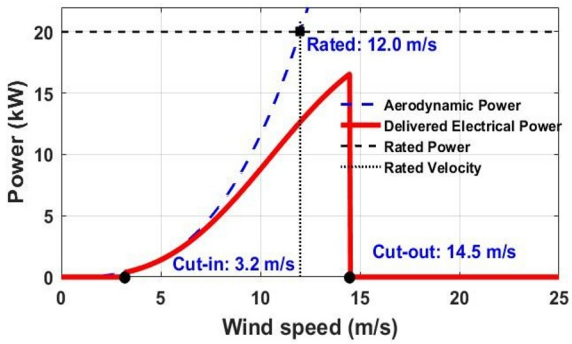

Fig. 6. DFIG wind turbine cut-in and cut-out characteristics.

Beyond this region, the power remains constant until the cut-out speed of 14.5 m/s, where the turbine disconnects for mechanical safety. This behavior confirms the appropriate aerodynamic design and DFIG control response integrated into the hybrid renewable microgrid system.

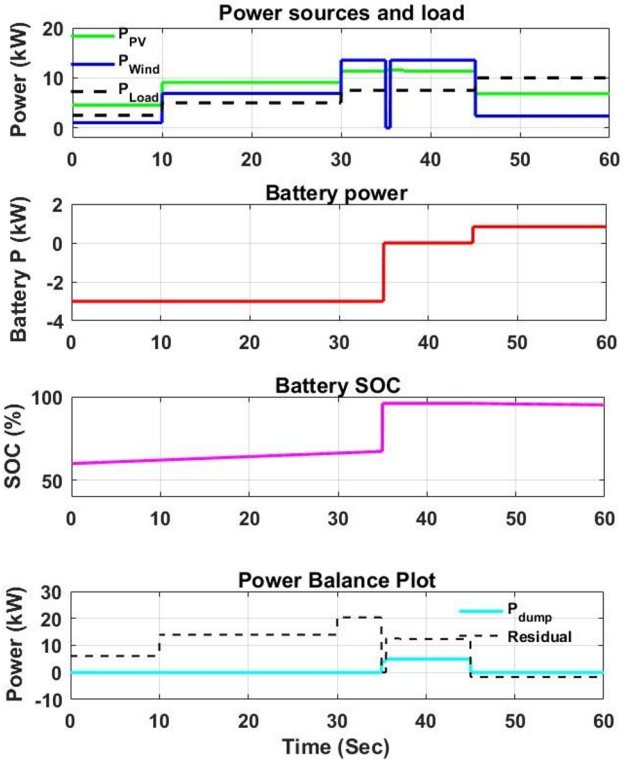

Fig. 7. Dynamic power flow characteristics of the integrated PV–wind–battery system showing DC dump-load activation.

The dynamic power response of the integrated wind–solar–battery system demonstrates that the coordinated energy management strategy maintains proper balance between generation and consumption under variable conditions as presented in Fig. 7. During low irradiance and wind speed, the total generation remains below the load demand, forcing the battery to discharge and stabilize the DC link. As the solar irradiance and wind velocity increase, the combined generation surpasses the load, and the excess power begins to charge the battery. This is reflected in a smooth charging phase, whereby the battery SOC rises from its initial value to the upper limit. If SOC reaches maximum limit, the ANN controller avoids over charging of the BESS. This change can be seen in the plateau at the 100% SOC point where the power at which charging take place levels of to zero hence proving the fact that the energy repository has reached its ideal capacity. The surplus energy is passed through a DC dump-load path once the charge on the battery is complete and the available generation is still beyond the total load. This auxiliary route will avoid the accumulation of energy in the DC bus, and thus maintain a stable voltage when using the system continuously.. The short activation of the dump load shown in the results corresponds to the over-generation period when the dump circuit absorbs the excess power that can no longer be stored in the battery. Such controlled energy diversion not only prevents over-current stress to both the converter and battery but also maintains steady voltage across the DC link. From the results, it is ensured that the proposed control logic acts only at the instance when the SOC crosses the defined threshold value with a short, stable dump-load pulse generation with no evidence of oscillation as depicted in Table 3. This confirms that the hybrid system effectively regulates the power flow within the renewable sources, storage element, and auxiliary dump path for system reliability and efficient utilization of the generated energy. From Table 3, it is observed that the ANN controller has reduced the current harmonics by 30% compared to the PI controller [4], [14].

Table 3. Comparison of THD values for PI and ANN Controllers

Controller	THD Before Filter (%)	THD After Filter (%)
PI	6.21	3.82
ANN	4.75	2.64

The results in Table 3 demonstrate that the ANN controller increases harmonic suppression by adjusting converter excitation dynamically, while the static nature of PI tuning cannot adapt during sudden environmental shifts.

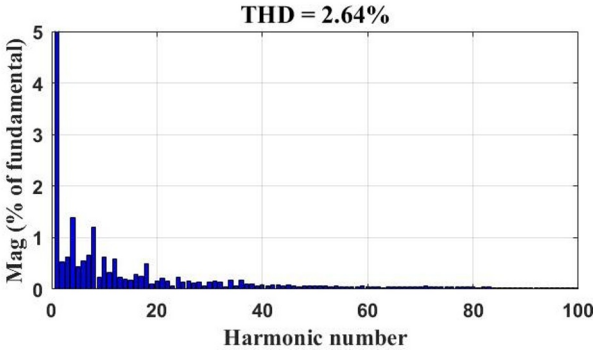

Fig. 8. FFT Spectrum of Load Current for Proposed ANN Controller.

Fig. 8. presents the harmonic spectrum of the load current obtained for the proposed ANN controlled inverter, where the dominant component appears at the 50 Hz fundamental frequency and all higher-order harmonics are effectively minimized. The observed THD of 2.64 % clearly shows the improved quality and reduced nonlinearity in the current achieved due to the adaptive learning characteristics of the ANN controller. The ANN, through an intelligent tuning of the controlling parameters in real time, provided smoothened current waveforms at the output, reduced switching losses, and advanced voltage regulation in contrast to the conventional PI-based approach. The harmonic content suppression consistently proves the stability and robustness of the proposed system under dynamic operating conditions. This chapter successfully demonstrated the capability of the ANN-based control strategy to reduce THD below IEEE standards and to enhance the performance of the inverter and the power quality of the hybrid renewable energy system, thereby validating the suitability of the proposed method for modern grid-interfaced applications. The post-filter THD of 2.64 % is very low compared to the 5 % limit set by IEEE 519 and can be compatible even with sensitive loads such as systems for communication and industrial control.

To assess the relative benefits of the intelligent controller, the same operational scenarios were simulated using both the conventional PI method and the ANN approach. The ANN consistently regulated the DC-link more tightly, limiting voltage fluctuations to within ±2%, whereas the PI controller produced non-negligible transient excursions when renewable sources changed abruptly. The harmonic response revealed a similar trend. Before filtering, the PI-based system exhibited higher distortion levels due to its fixed gains. After filtering, the ANN output maintained 2.64% THD compared to 3.82% for the PI controller. This reduction is attributed to the adaptive weight adjustments of the neural network which reduce overshoot and maintain synchronized duty modulation. The faster settling period of 0.08 s for the proposed controller confirms its ability to react effectively to rapid perturbations, which was not observed in the PI case.

5 Conclusion

The proposed artificial neural network–based adaptive controller demonstrated its capability to regulate the DC-link of a standalone hybrid microgrid under diverse and rapidly changing solar and wind conditions by intelligently coordinating power from renewable sources, battery storage, and the dump-load branch. Unlike fixed-gain proportional–integral control, the ANN continuously adjusts converter duty ratios and learns from system dynamics, which resulted in faster transient recovery, minimized overshoot, and lower harmonic distortion. The simulation outcomes underline this behavior, showing a voltage settling time of about 0.08 s and ripple constrained to around 3.2 V, while the total harmonic distortion reached 2.64%, comfortably satisfying IEEE 519 and IEEE 1547 criteria. These improvements demonstrate that the controller not only preserves bus stability during surplus and deficit power events but also enhances the utilization of renewable energy without compromising system reliability, and future work will extend this approach to hardware-based real-time implementation for long-term field validation.

References

1. A. K. Myla, S. R. Gorantla, Performance analysis of balanced integrated standalone microgrid under dynamic load conditions. J. New Mater. Electrochem. Syst. **26**(3), 155–163 (2023). https://doi.org/10.14447/jnmes.v26i3.a03
2. R. W. Kotla, S. R. Yarlagadda, Mathematical modeling of SPV array by considering the parasitic effects. SN Appl. Sci. **2**(1), 50 (2020). https://doi.org/10.1007/s42452-019-1861-x
3. H. C. Mohanta, B. T. Geetha, M. S. Alzaidi, I. S. Dhanoa, P. Bhambri, U. Mamodiya, R. Akwafo, An optimized PI controller-based SEPIC converter for microgrid-interactive hybrid renewable power sources. Wirel. Commun. Mobile Comput. 2022, 6574825 (2022). https://doi.org/10.1155/2022/6574825
4. N. Chettibi, A. Mellit, G. Sulligoi, A. M. Pavan, Adaptive neural network-based control of a hybrid AC/DC microgrid. IEEE Trans. Smart Grid **9**(3), 1667–1679 (2018). https://doi.org/10.1109/TSG.2016.2597006
5. R. W. Kotla, S. R. Yarlagadda, Comparative analysis of photovoltaic generating systems using particle swarm optimization and cuckoo search algorithms under partial shading conditions. J. Eur. Syst. Autom. **54**(1), 27–33 (2021). https://doi.org/10.18280/jesa.540104
6. B. Hamid, I. Hussain, S. J. Iqbal, B. Singh, S. Das, N. Kumar, Optimal MPPT and BES control for grid-tied DFIG-based wind energy conversion system. IEEE Trans. Ind. Appl. **58**(6), 7966–7977 (2022). https://doi.org/10.1109/TIA.2022.3202757
7. M. Rezkallah, S. Singh, A. Chandra, B. Singh, M. Tremblay, M. Saad, H. Geng, Comprehensive controller implementation for wind–PV–diesel-based standalone microgrid. IEEE Trans. Ind. Appl. **55**(5), 5416–5428 (2019). https://doi.org/10.1109/TIA.2019.2928254
8. Y. Sun, X. Hou, J. Yang, H. Han, M. Su, J. M. Guerrero, New perspectives on droop control in AC microgrid. IEEE Trans. Ind. Electron. **64**(7), 5741–5745 (2017). https://doi.org/10.1109/TIE.2017.2677328
9. F. Zhang, K. Thanapalan, A. Procter, S. Carr, J. Maddy, Adaptive hybrid maximum power point tracking method for a photovoltaic system. IEEE Trans. Energy Convers. **28**(2), 353–360 (2013). https://doi.org/10.1109/TEC.2013.2255292
10. S. Adiche, M. Larbi, D. Toumi, et al., Advanced control strategy for AC microgrids: a hybrid ANN-based adaptive PI controller with droop control and virtual impedance technique. Sci. Rep. **14**, 31057 (2024). https://doi.org/10.1038/s41598-024-82193-1
11. M. Liserre, F. Blaabjerg, S. Hansen, Design and control of an LCL-filter-based three-phase active rectifier. IEEE Trans. Ind. Appl. **41**(5), 1281–1291 (2005). https://doi.org/10.1109/TIA.2005.853373
12. D. Khan, K. Zhu, P. Hu, M. Waseem, E. M. Ahmed, Z. Lin, Active damping of LCL-filtered grid-connected inverter based on parallel feedforward compensation strategy. Ain Shams Eng. J. **14**(3), 101902 (2023). https://doi.org/10.1016/j.asej.2022.101902

13. M. Ali, A. A. Alhussainy, F. Hariri, S. Alghamdi, Y. A. Alturki, Performance assessment of current feedback-based active damping techniques for three-phase grid-connected VSCs with LCL filters. Mathematics **13**(16), 2592 (2025). https://doi.org/10.3390/math13162592
14. N. Wang, S. Zheng, W. Gao, Microgrid harmonic mitigation strategy based on the optimal allocation of active power and harmonic mitigation capacities of multi-functional grid-connected inverters. Energies **15**(17), 6109 (2022). https://doi.org/10.3390/en15176109
15. T. Pamulapati, M. Cavus, I. Odigwe, A. Allahham, S. Walker, D. Giaouris, A review of microgrid energy management strategies from the energy trilemma perspective. Energies **16**(1), 289 (2023). https://doi.org/10.3390/en16010289